SCIENTIFIC REPORTS

OPEN

Influence of rovibrational excitation on the non-diabatic state-to-state dynamics for the $Li(2p) + H_2 \rightarrow LiH + H$ reaction

Received: 5 October 2016
Accepted: 26 April 2017
Published online: 08 June 2017

Di He, Jiuchuang Yuan & Maodu Chen

The non-adiabatic state-to-state dynamics of the $Li(2p) + H_2 \rightarrow LiH + H$ reaction has been studied using the time-dependent wave packet method, based on a set of diabatic potential energy surfaces recently developed by our group. Integral cross sections (ICSs) can be increase more than an order of magnitude by the vibrational excitation of H_2, whereas the ICSs are barely affected by the rotational excitation of H_2. Moreover, ICSs of the title reaction with vibrationally excited H_2 decrease rapidly with increasing collision energy, which is a typical feature of non-threshold reaction. This phenomenon implies that the title reaction can transformed from an endothermic to an exothermic reaction by vibrational excitation of H_2. With the increase of the collision energy, the sideways and backward scattered tendencies of LiH for the $Li(2p) + H_2(v = 0, j = 0, 1) \rightarrow LiH + H$ reactions are enhanced slightly, while the backward scattering tendency of LiH for the $Li(2p) + H_2(v = 1, j = 0) \rightarrow LiH + H$ reaction becomes remarkably weakened. For the reaction with vibrationally excited H_2 molecule, both direct and indirect reaction mechanism exist simultaneously.

The reaction involving alkali atoms and H_2 molecule have been studied for decades[1–22]. Most of the researches focused on reactive collisions between ground state alkali atoms and hydrogen molecules[1–10]. However, only a few studies were devoted to reactions between electronically excited alkali metal atoms and H_2 molecules. The collision of excited alkali metal atoms with H_2 molecules can lead to a non-reactive quenching process or a reactive process. A diabatic transition is involved in both kinds of processes. Various experimental techniques have been used for investigating both classes of reactions[12–14]. Bililign *et al.*[11] applied the "half-collision" pump-probe technique to measure the far-wing absorption profiles of NaH_2 collision complex in the $Na(4^2P) + H_2$ reaction. In this experiment, the rotational state distributions of product NaH were observed. The $Cs(6D_{3/2}) + H_2 \rightarrow CsH + H$ reaction was studied in a crossed-beam experiment and CsH product was detected by laser-induced fluorescence[12]. Reaction cross sections and the rotational state distributions of CsH molecules were determined at the collision energy of 0.09 eV. Furthermore, the $K(5p^2P) + H_2 \rightarrow KH + H$ reaction was investigated by scattering state spectroscopic[13]. Rovibrational states populations of the KH product were determined from far-wing absorption spectra. The product nascent quantum state distributions of the $Rb(5^2D, 7^2S) + H_2 \rightarrow RbH + H$ reaction were determined by a laser pump-probe technique[14].

The $Li + H_2$ reaction is the simplest chemical reaction within this class of reactions which only involves an alkali atom and hydrogen molecule. Therefore, it is an ideal candidate for studying the reaction dynamics of this class of reactions. In 1987, Myers *et al.*[15] measured cross section of the $Li(2p) + H_2 \rightarrow LiH + H$ reaction at 788 K using absorption techniques. The quenching process during the $Li(3p) + H_2 \rightarrow Li(3s) + H_2$ was investigated under gas cell conditions[16]. Bililign *et al.*[17] studied the $Li(2p) + H_2 \rightarrow LiH + H$ reaction using the laser pump-probe far-wing scattering technique; the LiH product was observed when the collision energy was sufficiently high for the product formation. Furthermore, they found that reactive collisions take place preferentially in bent structure (near C_{2v} geometry). The influence of the vibrational excitation of H_2 reactant on the $Li(2p) + H_2 \rightarrow LiH + H$ reaction was studied by a pump-probe technique. Moreover, the rotational population distributions of LiH product were also obtained from the same experiment[18]. Up to now, the theoretical studies on the title reaction are still at

Key Laboratory of Materials Modification by Laser, Electron, and Ion Beams (Ministry of Education), School of Physics and Optoelectronic Technology, Dalian University of Technology, Dalian, 116024, P. R. China. Correspondence and requests for materials should be addressed to M.C. (email: mdchen@dlut.edu.cn)

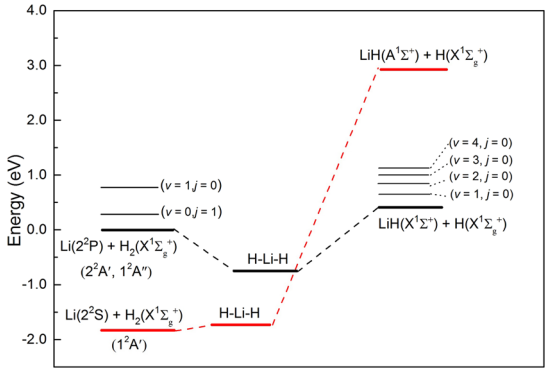

Figure 1. Schematic reaction path and energetic for the $Li(2p) + H_2 \rightarrow LiH + H$ reaction on the HYLC diabatic PESs.

a primary stage compared with the experimental studies. In 1997, Martinez performed a quantum mechanical nuclear dynamics for the $Li(2p) + H_2$ reaction and found that the non-adiabatic process was ultrafast[19]. Based on the adiabatic potential energy surfaces (PESs) of Li(2p, 3s, 3p) + H_2 system, Lee *et al.*[20] predicted the essential features of these reactions. The geometries of intermediates during the Li(2p, 3s) + H_2 reactions were examined in detail. In addition, they found that the reactive collision of the $Li(2p) + H_2 \rightarrow LiH + H$ reaction mainly occurs through a bent (C_{2v}) configuration. This conclusion is consistent with experimental results. However, the reaction dynamic calculations of the $Li(2p) + H_2 \rightarrow LiH + H$ reaction have not been conducted in Lee's study. Hsiao *et al.*[21] carried quasi-classical trajectory calculations on the $Li(2p) + H_2 \rightarrow LiH + H$ reaction based on two adiabatic PESs. The reactants correlate with the first exited state ($2^2A'$) adiabatic PES and the products correlate with the ground state ($1^2A'$) adiabatic PES. The influences of the vibrational excitation and collision energy on the title reaction were studied in their work. Moreover, the trajectories start from the first excited state $2^2A'$ and then hop to the ground state $1^2A'$ to form products at the exit channel. It should be noted that the transition probability between two adiabatic PESs was set to one, which is a simple approximation to treat the non-diabatic process during the $Li(2p) + H_2 \rightarrow LiH + H$ reaction. Recently, our group presented a set of diabatic PESs (HYLC PESs) using a diabatization scheme based on the transition dipole momentum operators for the title reaction[22]. The influence of collision energy on the reaction probability, integral cross section (ICS) and differential cross section (DCS) were studied based on the HYLC PESs using the time dependent wave packet (TDWP) method[22]. In the current work, in order to get detailed information on the influence of rovibrational excitations on the $Li(2p) + H_2 \rightarrow LiH + H$ reaction, the state-to-state dynamic of this reaction has been studied based on the HYLC PESs.

Results

Reaction probabilities. In order to conveniently analyze dynamic results within the framework of PESs, the schematic energy diagram of the title reaction is presented in Fig. 1 according to the HYLC PESs. As can be seen from Fig. 1, the energy of $Li(2p) + H_2(v = 1, j = 0)$ is higher than the that of $Li(2p) + H_2(v = 0, j = 1)$. The reaction probabilities of the reaction with different rovibrational states of the H_2 molecule and total angular momentum quantum numbers are depicted in Fig. 2 as a function of the collision energy. The three panels of Fig. 2 from (a) to (c) correspond to different rovibrational states of the reactant molecule at $H_2(v = 0, j = 0)$, $H_2(v = 0, j = 1)$, and $H_2(v = 1, j = 0)$ (hereinafter the same for the similar pictures). It can be seen that the reaction probabilities in Fig. 2(a) are similar to that in Fig. 2(b). In addition, it can be concluded that the reaction threshold of the $Li + H_2(v = 0, j = 0)$ reaction is slightly higher than that of $Li + H_2(v = 0, j = 1)$ reaction. As can be seen from the bottom panel of Fig. 2, the thresholds of the $Li(2p) + H_2 \rightarrow LiH + H$ reaction for total angular momentum quantum number J = 1 and J = 15 no longer exists when the reactant molecule is excited to the first vibrational excitation state.

The behavior of the reaction probability indicates that the rotational excitation has a small effect on the reactivity, while the vibrational excitation has a great influence on it. This is due to the fact that the energy released from the excited vibrational state $H_2(v = 1, j = 0)$ is much higher than the one which is released by the excited rotational state $H_2(v = 0, j = 1)$. It can be seen that the oscillations for the reactions with small total angular momentum are stronger than the one for the reactions with large total angular momentum. The reactions with small angular momentum prefer to take place in C_{2v} geometry (H-Li-H), which means the reactions are dominated by insertion mechanism. However, for the reactions with large total angular momentum, these reactions are dominated by abstraction mechanism. Moreover, we note that as the collision energies increase, the oscillations for reactions with small total angular momentum become unapparent. In all cases, the centrifugal barrier makes the threshold larger with the increase of the total angular momentum quantum number J.

Reaction cross sections. In the TDWP calculations, the maximum of total angular momentum quantum number J is 60, and the corresponding thresholds for the $Li(2p) + H_2(v = 1, j = 0)$ and $Li(2p) + H_2(v = 0, j = 1)$ reactions are 0.43 and 0.93 eV, respectively. Therefore, the upper limit of the collision energy in the calculations of ICSs and DCSs is set as 0.43 eV. The total ICSs of the $Li(2p) + H_2 \rightarrow LiH + H$ reaction with different initial rovibrational states of H_2 molecule as a function of collision energy are depicted in Fig. 3. The ICSs of the title reaction

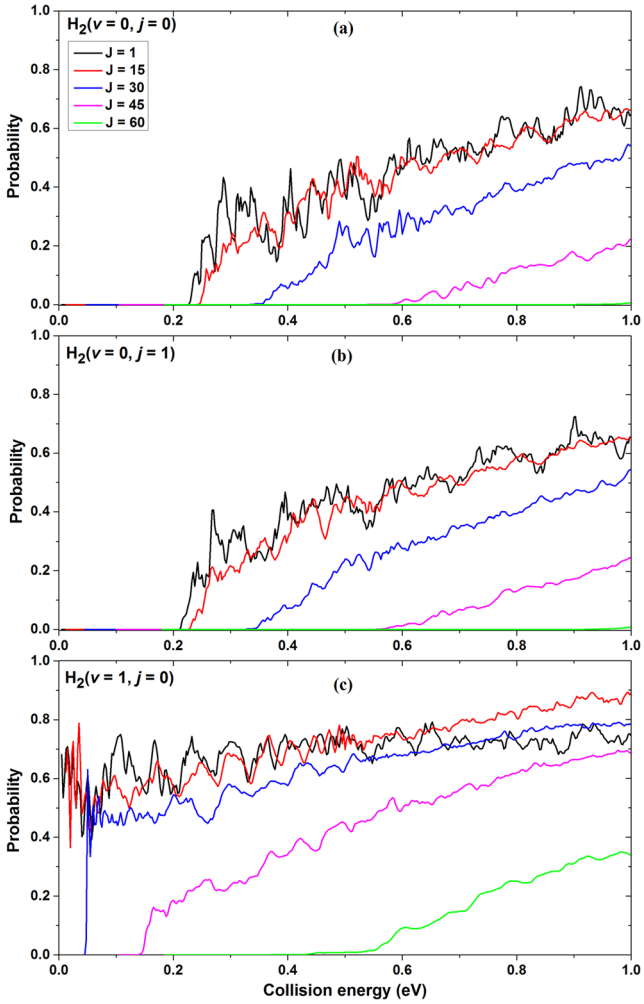

Figure 2. Reaction probabilities of the Li(2p) + $H_2 \rightarrow$ LiH + H reaction with (a) $H_2(v=0, j=0)$, (b) $H_2(v=0, j=1)$ and (c) $H_2(v=1, j=0)$ as a function of collision energy.

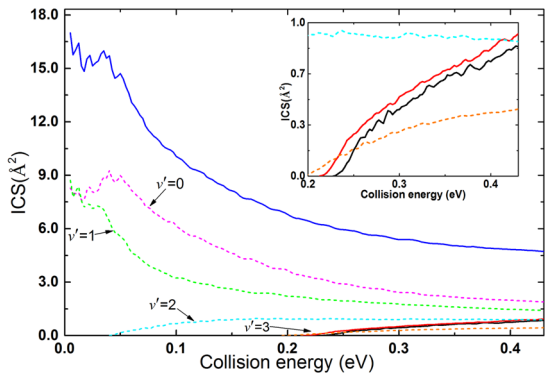

Figure 3. Total ICSs of the Li(2p) + $H_2 \rightarrow$ LiH + H reaction for different initial rovibrational states of H_2 molecule and product vibrationally resolved ICSs of the Li(2p) + $H_2(v=1, j=0) \rightarrow$ LiH($v'=0, 1, 2, 3$) + H reaction. Black, red and blue solid lines stand for $H_2(v=0, j=0)$, H_2 $(v=0, j=1)$ and $H_2(v=1, j=0)$, respectively. Magenta, green, cyan and orange dash lines stand for $v'=0$, 1, 2 and 3 respectively.

with $H_2(v=0, j=0)$ and $H_2(v=0, j=1)$ are quite lower than the one of $H_2(v=1, j=0)$ over the whole collision energy range. At low collision energies, the ICS for $H_2(v=1, j=0)$ starts from a high value and then decreases rapidly with increasing collision energy, which is a typical feature of barrierless reactions. Due to the fact that the

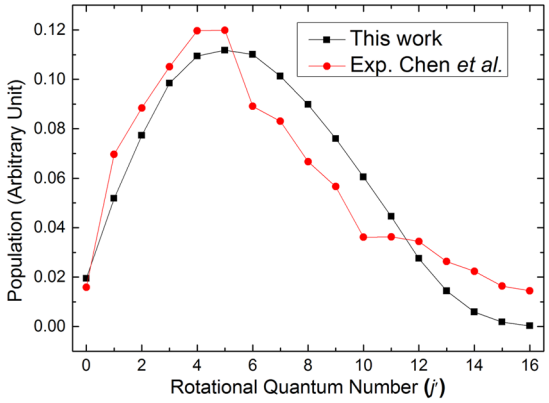

Figure 4. Comparison of rotational state distributions of the LiH products for the Li(2p) + $H_2(v=0, j=1)$ reaction between the theoretical and experimental results over the whole calculated collision energies ($0.0025 < E_{col}/eV < 0.43$)[18].

potential energy of Li(2p) + $H_2(v=1, j=0)$ reactants is higher than the potential energy of LiH($v'=0, 1$) + H products as we observed in Fig. 1. In addition, we have found that the reaction process of the Li(2p) + H_2(v = 1, j = 0) reaction is similar to the reaction processes of N(^{2}D) + H_2 and O(^{1}D) + H_2 reactions[23]. At low collision energies ($E_{col} < 0.05$ eV), the Li(2p) + $H_2(v=1, j=0)$ reaction is dominated by insertion mechanism leading to a long-lived intermediate complex which make a significant contribution to the oscillations in the ICS. At relatively high collision energies ($E_{col} > 0.05$ eV), the available energy is sufficient large for the reactants to surmount the centrifugal barrier and escape the potential well within a short time interval. The Li(2p) + $H_2(v=1, j=0)$ reaction is dominated by direct abstraction mechanism resulting in the absence of oscillations in the ICS over the collision energies of 0.05 to 0.43 eV.

In contrast, the ICSs for the Li(2p) + $H_2(v=0, j=0, 1)$ reactions increase monotonically with an increase of collision energy. Furthermore, it is observed that the rotational excitation of H_2 molecule has small influence on the ICSs. Clearly, the vibration excitation of the H_2 molecule has greater impact on the ICSs than the rotation excitation of H_2 molecule, which is caused by the fact that the internal energy of $H_2(v=1, j=0)$ molecule is much larger than that of $H_2(v=0, j=1)$. To get information about the vibrational states of LiH products, the products vibrationally resolved ICSs of the Li(2p) + $H_2(v=1, j=0) \rightarrow$ LiH($v'=0, 1, 2, 3$) + H reaction are also presented in Fig. 3. However, the products vibrationally resolved ICSs of the Li(2p) + $H_2(v=0, j=0, 1)$ reactions are not presented in this figure due to the fact nearly all of the LiH products of the two reactions distribute in vibrational ground state. At low collision energies ($E_{col} \leq 0.05$ eV), a few oscillations appears on the ICSs curves of LiH($v'=0$, 1), which are similar to the results observed from the Ne + H_2^+reaction[24,25]. In addition, we found the reaction path of the Ne + $H_2^+ \rightarrow NeH^+ + H$ reaction is similar to the one of the title reaction. The oscillations on the ICSs of the Li(2p) + $H_2(v=1, j=0)$ reaction are probably induced by the resonances arising from of unstable H-Li-H complex, which resembles to the situation found in the Ne + $H_2^+ \rightarrow NeH^+ + H$ reaction[24].

Vibrational and rotational state distributions. To verify the reliability of our dynamic results, a comparison for the rotational state distribution of the LiH products of the Li(2p) + $H_2(v=0, j=1)$ reaction between the theoretical and experimental results is presented in Fig. 4[18]. In order to make the theoretical results conform to the actual situation, the Maxwell speed distribution is considered in the theoretical results. The arbitrary unit is employed in the experiment, thus it is necessary to scale the experiment data to our theoretical results. In this work, both the sums of relative rotational populations of experimental and theoretical results are set to one. As can be seen from Fig. 4, the rotational state distribution of the theoretical results is in reasonable agreement with the experimental results, except for the range in which the rotational quantum number j is larger than 6. Owing to the fact that the H_2 molecule is consisted of about 67% $H_2(v=0, j=1)$, 22% $H_2(v=0, j=3)$ and a small amount of $H_2(v=0, j=0, 2)$ molecules in Chen's experiment, however, only the case with $H_2(v=0, j=1)$ was involved in the theoretical results of Fig. 4. In general, the trend of theoretical results is consistent with the experimental one, which validating the accuracy of our calculations.

In order to gain detailed information about the internal state distributions of the LiH product molecule, the vibrational state and rotational state distributions of LiH molecule are depicted in Figs 5 and 6, respectively. Figure 5 clearly shows that nearly all LiH product distributed in $v'=0$ state for the Li(2p) + $H_2(v=0, j=0, 1)$ reactants indicate that the rotational excitation ($j=1$) of H_2 molecule has a little influence on the vibrational state distributions of LiH product. At the same time, only a small fraction of LiH products distribute in $v'=1$ state for the Li(2p) + $H_2(v=0, j=0, 1)$. Over the whole calculated collision energies ($0.0025 \leq E_{col}/eV \leq 0.43$), the LiH molecule cannot be excited to higher vibrational level than $v'=1$ for the Li(2p) + $H_2(v=0, j=0, 1)$ reactions. In contrast, the product LiH molecule distribute in four vibrational levels (from $v'=0$ to $v'=3$) for the Li(2p) + $H_2(v=1, j=0)$ reaction. More specifically, the LiH products are mainly generated in the ground vibrational state and the vibrational state distributions decrease gradually with the increase of vibrational quantum number. The vibrational state distribution of LiH products can be interpreted by taking into account the energy gap between reactants and products. As shown in Fig. 1, the product channel to highly excited vibrational state

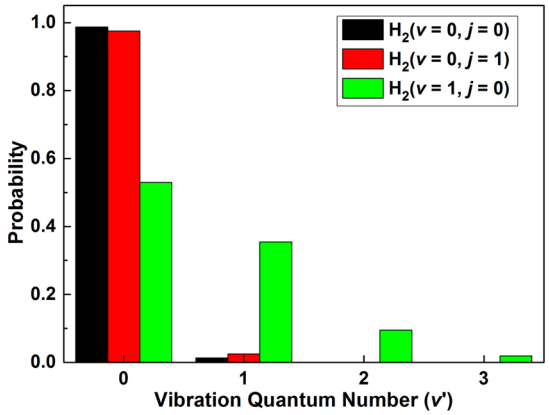

Figure 5. Vibrational state distributions of LiH molecules in the $Li(2p) + H_2 \rightarrow LiH + H$ reaction for different initial rovibrational states of H_2 molecule over the whole calculated collision energies ($0.0025 < E_{col}/eV < 0.43$).

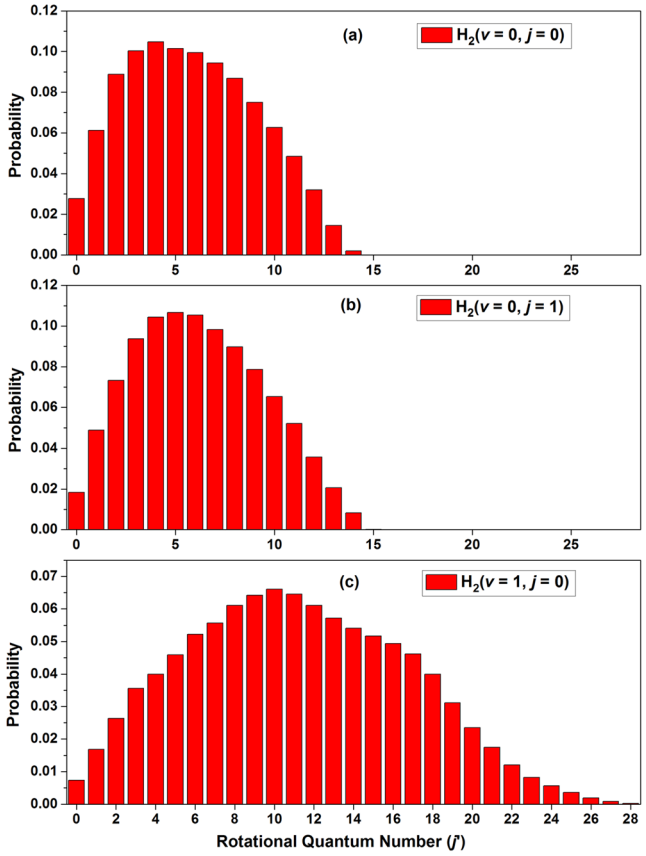

Figure 6. Rotational state distributions of LiH molecules in the $Li(2p) + H_2 \rightarrow LiH + H$ reaction for different initial rovibrational states of H_2 molecule over the whole calculated collision energies ($0.0025 < E_{col}/eV < 0.43$). (**a**) $H_2(v=0, j=0)$; (**b**) $H_2(v=0, j=1)$; (**c**) $H_2(v=1, j=0)$.

LiH molecule can be opened easily for the $Li(2p) + H_2(v=1, j=0)$ reactants with increasing collision energy. However, the product channel $LiH(v'=2) + H$ is accessible for the $Li(2p) + H_2(v=0, j=1)$ reactants until the collision energy larger than 0.52 eV. In addition, the potential well located in the reaction path has important effect on the energy distribution of products. There are lots of bound and quasi-bound states in the intermediate complex, which is conducive to the distribution of available energy on the rovibrational states of product.

To obtain detailed information about the energy distribution, the rotational state distributions of LiH molecules are shown in Fig. 6 as a function of collision energies in the range of 0.0025 to 0.43 eV. The shape of the rotational state distributions for the $Li(2p) + H_2(v=0, j=0)$ reaction is similar to that of $Li(2p) + H_2(v=0, j=1)$ reaction. Moreover, the peaks of the rotational state distribution of LiH product for the reaction with $H_2(v=0,$

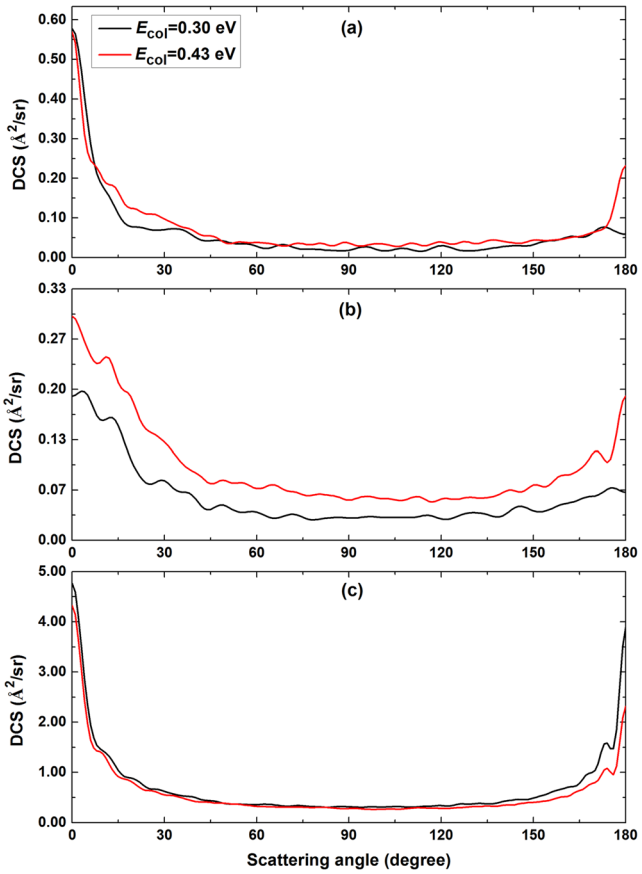

Figure 7. Total DCSs of the Li(2p) + $H_2 \rightarrow$ LiH + H reaction at two collision energies of 0.30 and 0.43 eV. (**a**) $H_2(v=0, j=0)$; (**b**) $H_2(v=0, j=1)$; (**c**) $H_2(v=1, j=0)$.

$j=0$) and $H_2(v=0, j=1)$ are $j'=4$ and $j'=5$, respectively. Comparing the middle panel with the bottom panel of Fig. 6, we can see that the upper limit of rotational quantum number of LiH product for the Li + $H_2(v=0, j=1)$ reaction is $j'=15$, while the one for the Li + $H_2(v=1, j=0)$ reaction is $j'=28$. Another important feature in bottom panel of Fig. 6 is that the peak of the rotational distribution of LiH product is $j'=10$ which is larger than these of the Li(2p) + $H_2(v=0, j=0, 1)$ reactions. In all cases, the percentage of the rotational level population of the LiH product increases rapidly before reaching peak, and then decreases gradually with the increase of the rotational quantum number. For the reaction Li + $H_2(v=1, j=0)$, the reaction is dominated by abstraction mechanism gradually with the increase of collision energy, which means this reaction prefer to form a H-H-Li intermediate complex rather than a H-Li-H intermediate complex. In this this case, the energy released by the $H_2(v=1, j=0)$ more likely to transform to the rotational energy of LiH.

Differential cross sections. Figure 7 shows the DCSs for the title reaction at two collision energies of 0.30 and 0.43 eV. The three panels from (a) to (c) correspond to different initial rovibrational states of H_2 reactant. Despite the variation trends of the DCSs with increasing collision energy are different, the DCSs in the three panels show a forward scattering ($0° < \theta < 60°$) tendency. From the upper panel of Fig. 7, it is clearly seen that the LiH product molecules for the Li(2p) + $H_2(v=0, j=0)$ reaction are scattered mainly in the forward hemisphere at the both collision energies. Only few LiH products scatter at the sideways ($60° < \theta < 120°$). In addition, it is observed that more and more the LiH product molecules prefer to scatter at the backward hemisphere ($120° < \theta < 180°$) with increasing collision energy. As shown in the middle panel of Fig. 7, the forward and the sideways scattering are enhanced gradually with increasing collision energy. At the same time, the increased degree of LiH molecules scattering at backward direction are more than these scattering at forward direction. Since the energy level of the LiH($v'=0$) + H products is higher than the energy levels of Li(2p) + $H_2(v=0, j=0, 1)$ reactants, long-lived complexes cannot be converted into LiH + H products efficiently at low collision energy of 0.3 eV. In this case, the products are yielded by reactions with single collision and the energies released by $H_2(v=0, j=0, 1)$ have a small influence on the scattering direction of LiH molecule, the scattering direction of product molecule is mainly determined by the velocity of incoming atom. This mechanism leads to that the DCSs of the Li(2p) + $H_2(v=0, j=0, 1)$ reactions are governed by forward scattering at low collision energies. At collision energy of 0.43 eV, more and more LiH + H products are formed by long-lived complexes which will reduce the effect of velocity of the incoming atom by its chaotic rovibration motions. This mechanism leads to the angular distribution isotropic, i.e., the DCS symmetric with respect to $\theta = \pi/2$[26,27]. It appears as the significant enhancement of the backward peaks of the DCSs for the Li + $H_2(v=0, j=0, 1)$.

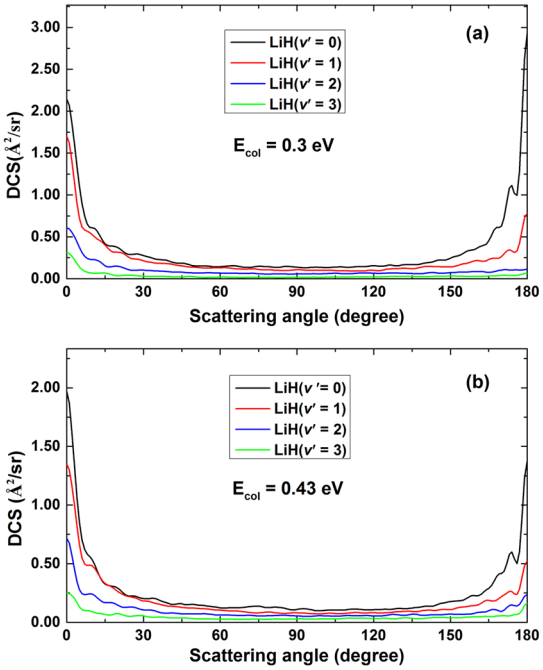

Figure 8. The products vibrationally resolved DCSs of the Li(2p) + $H_2(v=1, j=0) \rightarrow$ LiH($v'=0, 1, 2, 3$) + H reactions at two collision energies.

In contrast to the influence of rotational excitation of the H_2 on ICSs, the rotational excitation of the H_2 reactant molecule has a significant effect on the DCSs of the title reaction. Comparing the upper panel with the middle panel of Fig. 7, it is found that the difference among the forward, sideways and backward scattering is reduced when the H_2 reactant molecule is excited to the first rotationally excited state from ground state. The trend of forward scattering peak of LiH molecule as angular momentum j increase of reactant molecule is similar to the results obtained from the $D^+ + H_2$ reaction[27]. The polarization peaks (peak close to 0° an 180°) are contributed by the collisions with $K = K_0 = 0$, where K and K_0 are the projection quantum number of the diatom rotational state onto the initial and final relative translational velocity vectors, respectively. The statistical weight $[1/(2j_0 + 1)]$ of the collisions with $K = K_0 = 0$ decreases as the increases of the angular momentum of H_2[27], thus the forward and backward scattering peaks decrease with the increase of the rotational excitation of H_2. In comparison with the middle panel of Fig. 7, the bottom panel exhibits opposite behavior. The DCSs for the Li(2p) + $H_2(v=1, j=0)$ reaction decrease with the increase of the collision energy, especially the backward scattering decrease rapidly as the collision energy increases. Obviously, the DCSs of the Li + $H_2(v=1, j=0)$ reaction is dominated by the forward scattering with increasing collision energy. It reveals that the direct mechanism becomes more prevalent for the title reaction with $H_2(v=1, j=0)$ with increasing collision energy. In order to gain additional insight into the reaction dynamics of the title reaction, the products vibrationally resolved DCSs of the Li(2p) + $H_2(v=1, j=0) \rightarrow$ LiH($v'=0, 1, 2, 3$) + H reaction are presented in Fig. 8. The products vibrationally resolved DCSs of the Li(2p) + $H_2(v=0, j=0, 1)$ reactions are not presented in this work since the LiH products of these two reactions are almost entirely distributed in vibrational ground state. For the results of LiH($v'=0$), both forward and backward scattering can be observed at the two collision energies of 0.3 and 0.43 eV. It is notable that the scattering angle corresponding to the maximum of the DCS of LiH($v'=0$) is changing from $\theta = 180°$ to $\theta = 0°$ with the increase collision energy. Comparing the DCS of LiH($v'=1$) in Fig. 8(a) with the one in Fig. 8(b), the degree of forward scattering is enhanced as the collision energy increases. It is due to that the direct mechanism is more prevalent for the Li(2p) + $H_2(v=1, j=0) \rightarrow$ LiH($v'=1$) + H reaction at relatively high collision energies. The backward scatterings of the DCSs for LiH($v'=2, 3$) are more pronounced at collision energy of 0.43 eV than these at collision energy of 0.3 eV. This reveal that more and more long-lived complexes transform into highly excited vibrational LiH($v'=2, 3$) products. In other words, the direct and indirect mechanism exist in the Li(2p) + $H_2(v=1, j=0) \rightarrow$ LiH + H reaction simultaneously over the collision energies range of 0.3–0.43 eV.

To obtain deeply understanding about the reaction mechanism of the title reaction, the state-to-state DCSs at two collision energies of 0.30 and 0.43 eV are calculated. Only the DCSs of LiH($v'=0$) products are presented in Fig. 9 due to the fact that most of the LiH product molecules are distributed in ground vibrational state. The left and right panels show the DCSs for $E_{col} = 0.30$ eV and $E_{col} = 0.43$ eV, respectively. The left panels from (a) to (c) correspond to the reactant molecule at $H_2(v=0, j=0)$, $H_2(v=0, j=1)$ and $H_2(v=1, j=0)$, and the same to the right panels from (d) to (f). By comparing Fig. 9(a) with Fig. 9(d), it can be concluded that the DCSs for LiH($v'=0$) at the two collision energies are dominated by forward scattering, and the backward scattering at collision energy of 0.30 eV can be ignored. In addition, the backward scattering peak for $E_{col} = 0.43$ eV is contributed by lowly excited rotational LiH products. For the Li(2p) + $H_2(v=0, j=0)$ reaction, long-lived complexes cannot be transformed into LiH + H products efficiently at collision energy of 0.3 eV. With increasing collision energy,

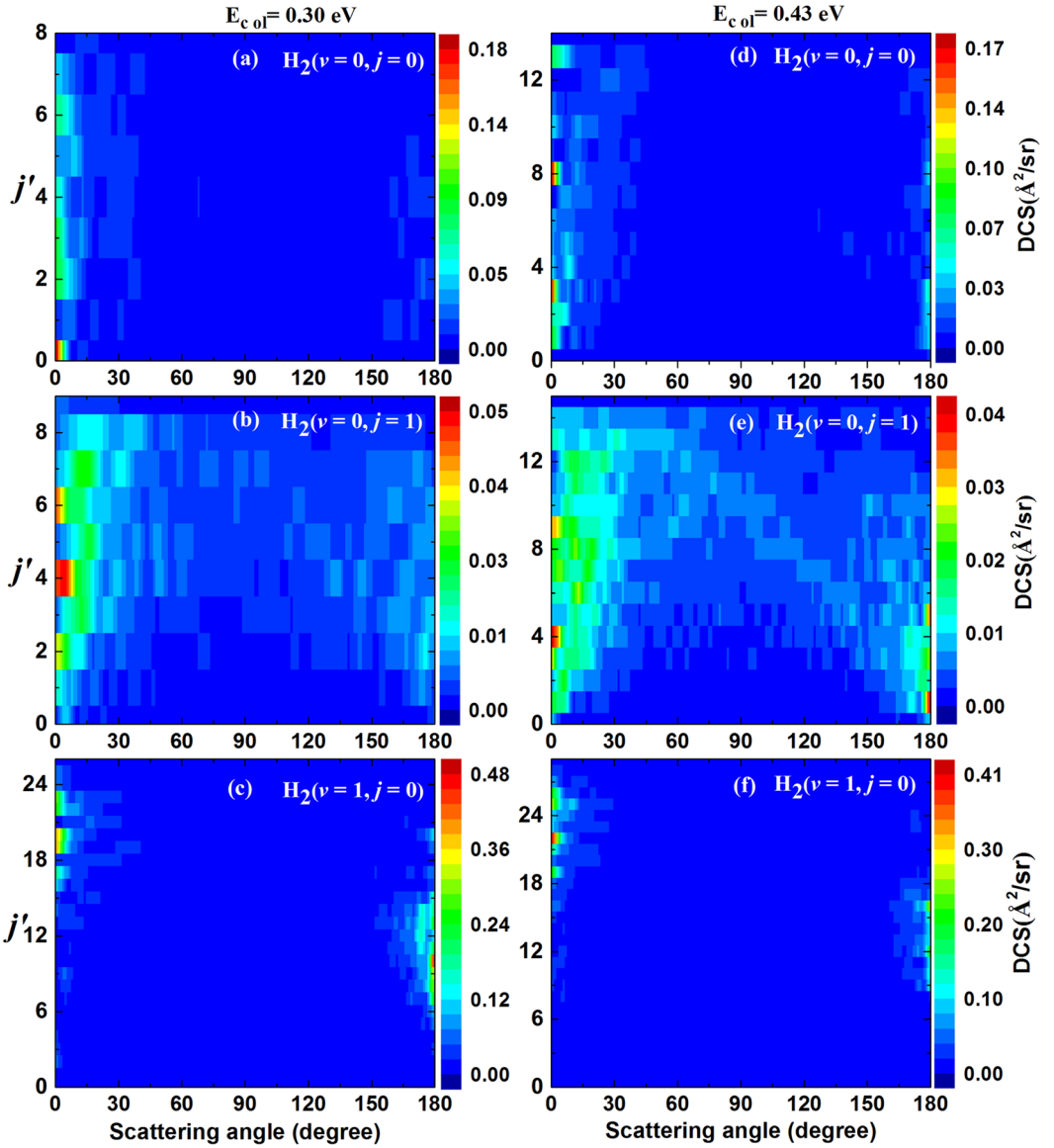

Figure 9. State-to-state DCSs(Å^2/sr) of the Li(2p) + H_2 → LiH + H reaction for different initial rovibrational states of H_2 molecule. Left panels: at collision energy of 0.30 eV; right panels: at collision energy of 0.43 eV.

a small number of long-lived complexes with low internal energy can be converted into products, thus the backward scattering is mainly contributed by rotationally lowly excited LiH molecules. It is clearly seen from the upper panels and the middle panels of Fig. 9 that the sideways scattering is enhanced while the H_2 reactant is excited to first rotationally excited state.

As can be seen from the bottom panels of Fig. 9, the forward and backward peaks of the DCSs distributed in different range of j'. The forward peaks distribute in large rotational quantum number j' and the backward peaks distribute in relatively small rotational quantum number j'. The state-to-state DCSs exhibit an asymmetrical feature, which is a typical characteristic of direct reaction. The backward peaks of the DCSs are mainly contributed by the reactive collisions with large total angular momentum and the forward peaks of the DCSs are mainly contributed the reactive collision with small total angular momentum. To further explain the reaction mechanism of the Li(2p) + $H_2(v=1, j=0)$ → LiH + H reaction more clearly, the differential cross sections (DCSs) of the Li(2p) + $H_2(v=1, j=0)$ → LiH + H reaction for different total angular momentum presented have been analyzed in Fig. 10. It is shown that the DCSs forward peaks are mainly contributed by reactive collisions with small total angular momentum ($J \leq 39$). At the same time, the DCSs backward peaks are mainly contributed by reactive collisions with relatively larger total angular momentum ($J \geq 40$). The forward and backward peaks are distributed in different range of total angular momentum, which means the Li(2p) + $H_2(v=1, j=0)$ → LiH + H reaction is dominated by direct reaction mechanism rather than complex-forming mechanism.

The Li atom collides with the H_2 molecule with large total angular momentum, and the centrifugal barrier makes the reaction path of the Li(2p) + $H_2(v=1, j=0)$ reaction similar to the one which take place on a repulsive

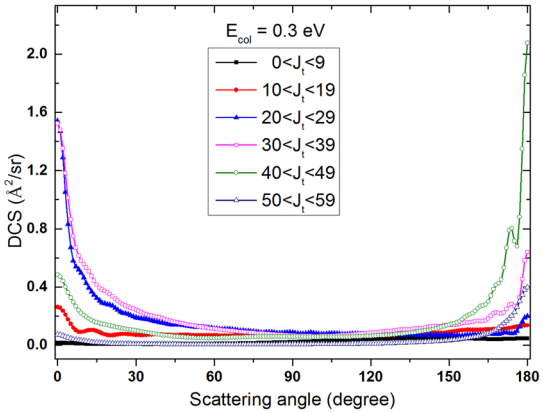

Figure 10. DCSs of the Li(2p) + $H_2(v=1, j=0)$ → LiH + H reaction for different total angular momentum J at collision energy of 0.30 eV.

Grid/basis range and size	$R \in$ [0.01 a.u., 15.0 a.u.], $N_R = 149$
	$r \in$ [0.01 a.u., 15.0 a.u.], $N_R = 149$
	$j_{min} = 0 \sim j_{max} = 69$, $N_j = 69$ over [0°,180°]
Initial wave -packet	$R_0 = 10.0$ a.u.
$\exp\left[-\frac{(R-R_0)}{2\Delta_R^2} ik_0 R\right]$	$\Delta_R = 0.08$ a.u.
	$k_0 = (2E_0\mu_R)^{1/2}$ with $E_0 = 0.5$ eV
Absorption functions for $H_2(v=1, j=0)$	$\exp[-0.0192 \times \Delta_t(r-12.5)^2]$, for $12.5 \le r \le 15.0$
	$\exp[-0.016 \times \Delta_t(R-12.5)^2]$, for $12.5 \le R \le 15.0$
Absorption functions for $H_2(v=0, j=0, 1)$	$\exp[-0.0192 \times \Delta_t(r-12.5)^2]$, for $12.5 \le r \le 15.0$
	$\exp[-0.0144 \times \Delta_t(R-12.5)^2]$, for $12.5 \le R \le 15.0$
Total propagation time	40000 a.u.
Time step	15 a.u.
Highest J Value	60

Table 1. Numerical Parameters used in the TDWP calculations.

PES. The $H_2(v=1, j=0)$ molecule start to release its internal energy till the Li atom close to the H_2 molecule in this case. Most of the energy released by the $H_2(v=1, j=0)$ molecule turns into translational energy of products, and only a little energy released by reactants converted into the internal energy of LiH products. Therefore, the LiH products with relatively low rotational states exhibit evident backward scattering tendency. In contrast, the forward scattering LiH products with rotationally highly excited states are mainly contributed by these reactions with small total angular momentum. The $H_2(v=1, j=0)$ molecule start to release its internal energy when the Li atom towards to H_2 molecule in this case. Most of the internal energy of the reactants are converted into the rotational energy of LiH products, hence, the velocity of the LiH molecules nearly parallel to the velocity direction of the incoming Li atom. This mechanism has mainly contributed to forward scattering tendency of rotationally highly excited LiH molecule. These behaviours are in agreement with the analyses of Polanyi[28].

Discussion

The influence of the rovibrational excitation of H_2 molecule on the Li(2p) + H_2 → LiH + H has been investigated using a set of diabatic PESs constructed by our group[22]. The vibrational excitation of H_2 reactant has greater influence than the rotational excitation on the reaction probability and ICS of the title reaction due to the fact that the energy released by the vibrationally excited $H_2(v=1, j=0)$ is larger than the one released by the rotationally excited $H_2(v=0, j=1)$. The threshold energy on the curves of reaction probability and ICS are eliminated when the H_2 reactant molecule is excited to the first excited vibrational states, which indicate the endothermicity of the reaction can be overcome by the energy released from the internal energy of $H_2(v=1, j=0)$ molecule. The vibrational and rotational state distributions of LiH product reveal that the internal energy of the $H_2(v=1, j=0)$ reactant could be transformed into internal energy of LiH product effectively. The results of DCSs show that the angular distribution of the LiH product molecule is dominated by forward scattering. The rotational excitation, vibrational excitation and collision energy of reactants have different effects on the DCSs. Comparing the DCSs of the Li(2p) + $H_2(v=0, j=0)$ reaction with the DCSs of the Li(2p) + $H_2(v=0, j=1)$ reaction, the rotational excitation of H_2 molecule enhances the sideways and backward scattering of LiH products. The microscopic mechanism of the Li(2p) + $H_2(v=1, j=0)$ reaction is very complicated. More specifically, the direct reaction mechanism dominates the Li(2p) + $H_2(v=1, j=0)$ → LiH($v=0$) + H reaction, and the direction of the vibrationally lowly excited LiH($v=0$) product is very sensitive to the total angular momentum of the reactants. In addition,

both direct and indirect reaction mechanism exist simultaneously for the reactions with vibrationally highly excited LiH($v = 1, 2, 3$) products. Otherwise, for the reaction with vibrationally excited H_2 molecule, the forward scattering of LiH products is enhanced with increasing collision energy. In general, the scattering behaviour of the title reaction can be attributed by a competition between the two different reaction mechanisms.

Methods

Diabatic Potential Energy Surfaces. The diabatic PESs (HYLC PESs) employed here are constructed based on 30,796 high-level *ab initio* energy points which are calculated by multi-reference configuration interaction calculations using basis sets of quadruple zeta quality. The diabatic potential energies are obtained from the diabatization scheme based on transition dipole momentum operators. The neural network method was used for fitting the diabatic PESs. As far as we know, it is the most accurate diabatic PESs for the title reaction to date. Figure 1 depicts the schematic energy diagram of the title reaction according to the HYLC PESs. There is a potential well about 0.8 eV along the reaction path due to the surface crossing between the two coupled states. The potential well located in the entrance channel has a great influence on the reaction dynamics of title reaction, especially at the low collision energy range. More details of the HYLC PES can be found in Ref. 22.

Dynamical Calculations. The TDWP method has been successfully applied to study the reaction dynamics in many reactive systems[29–35]. The theory of the TDWP method has been extensively described in previous work[36,37]. Here, we only introduce the outline of the TDWP method. The TDWP method employed in this study is developed by Sun *et al.*, which only requires the wave-packet propagate in reactant Jacobi coordinates to extract the *S*-matrix information. This method is fairly effective in dealing with the reaction, which takes place over two coupled PESs, such as the $Cl + H_2$ reaction[32]. In the body fixed representation, the Hamiltonian of the $Li(2p) + H_2$ system can be written as

$$\hat{H} = \hat{H}_0 + \hat{U}, \tag{1}$$

where

$$\hat{H}_0 = -\frac{\hbar^2}{2\mu_R}\frac{\partial^2}{\partial R^2} + \hat{h}(r), \tag{2}$$

$$\hat{U} = \frac{(\hat{J} - \hat{j})^2}{2\mu_R R^2} + \frac{\hat{j}^2}{2\mu_r r^2} + \hat{V}^d = \hat{V}_{rot} + \hat{V}^d. \tag{3}$$

Here, $\hat{h}(r)$ is the diatom reference potential. R is the vector from Li atom to the mass center of the H_2 molecule and r is the vibrational vector of the H_2 molecule, μ_R and μ_r acre the corresponding reduced masses. J and j are total angular momentum operator of the LiH_2 system and rotational angular momentum operator of reactant diatomic molecule, respectively. $\hat{V}^d$ is a 2×2 matrix which represents the potential energy of the LiH_2 system. The split operator method was employed in the propagation of the wave function:

$$\begin{bmatrix}\psi_1(t+\Delta_t)\\ \psi_2(t+\Delta_t)\end{bmatrix} = e^{-iH_0\Delta_t/2}e^{-iV_{tot}\Delta_t/2}e^{-i\begin{bmatrix}V_{11}^d & V_{12}^d\\ V_{21}^d & V_{22}^d\end{bmatrix}\Delta_t}e^{-iV_{tot}\Delta_t/2}e^{-iH_0\Delta_t/2}\begin{bmatrix}\psi_1(t)\\ \psi_2(t)\end{bmatrix}. \tag{4}$$

The diabatic potential matrix $\hat{V}^d$ can be transformed to adiabatic potential matrix $\hat{V}^a$ using the diabatic-to-adiabatic transformation matrix T

$$\begin{bmatrix}V_1^a & 0\\ 0 & V_2^a\end{bmatrix} = T\begin{bmatrix}V_{11}^d & V_{12}^d\\ V_{21}^d & V_{22}^d\end{bmatrix}\widetilde{T}^+. \tag{5}$$

According to the Eq. (5), the Eq. (4) can be written as

$$\begin{bmatrix}\psi_1(t+\Delta_t)\\ \psi_2(t+\Delta_t)\end{bmatrix} = e^{-\frac{iH_0\Delta_t}{2}}e^{-\frac{iV_{tot}\Delta_t}{2}}T\begin{bmatrix}e^{-iV_1^a\Delta_t} & 0\\ 0 & e^{-iV_2^a\Delta_t}\end{bmatrix}\widetilde{T}^+ \times e^{-iV_{tot}\Delta_t/2}e^{-iH_0\Delta_t/2}\begin{bmatrix}\psi_1(t)\\ \psi_2(t)\end{bmatrix}, \tag{6}$$

The reactant-coordinate-based method is used to extract the state-to-state *S*-matrix. The state-to-state reaction probability is obtained by

$$P_{vj\leftarrow v_0 j_0}^J = \frac{1}{2j_0+1}\sum_{K,K_0}\left|S_{vjK\leftarrow v_0 j_0 K_0}^J\right|^2. \tag{7}$$

The state-to-state ICS is given by

$$\sigma_{vj\leftarrow v_0 j_0} = \frac{\pi}{(2j_0+1)k_{v_0 j_0}^2}\sum_K\sum_{K_0}\sum_J(2J+1)\left|S_{vjK\leftarrow v_0 j_0 K_0}^J\right|^2, \tag{8}$$

The state-to-state DCS can be calculated by the following equation:

$$\frac{d\sigma_{vj\leftarrow v_0 j_0}(\theta, E)}{d\Omega} = \frac{1}{(2j_0 + 1)}\sum_K\sum_{K_0}\left|\frac{1}{2ik_{v_0 j_0}}\sum_J(2J + 1)d^J_{KK_0}(\theta)S^J_{vjK\leftarrow v_0 j_0 K_0}\right|^2, \quad (9)$$

in which the θ is the scattering angle between the incoming Li(2p) + H_2 reactants and the scattered LiH + H products. The Wigner function $d^J_{KK_0}(\theta)$ is used for calculating the reduced rotation matrix element. In order to consider the effect of the centrifugal potential operator properly, the full Coriolis-coupled are involved in the TDWP calculations. In this study, the rovibrational states of H_2 molecule are set as ($v = 0, j = 0$), ($v = 0, j = 1$) and ($v = 1, j = 0$) for investigating the influence of the rovibrational excitation. The numerical parameters used in this calculations aresummarized in Table 1, the different numerical parameters for different initial states of H_2 molecules are also presented in this table.

References

1. Dunne, L. J., Murrell, J. N. & Jemmer, P. Analytical potential energy surface and quasi-classical dynamics for the reaction LiH(X, $^1\Sigma^+$) + H(^{2}S) → Li(^{2}S) + H_2(X, $^1\Sigma_g^+$). *Chem. Phys. Lett.* **336**, 1–6 (2001).
2. Berriche, H. & Tlili, C. Ab initio potential energy surface and rotationally inelastic collisions of LiH ($X^1\Sigma^+$) with H. I. The ab initio evaluation of the potential energy surface. *J. Mol. Struct.: THEOCHEM* **678**, 11–16 (2004).
3. Padmanaban, R. & Mahapatra, S. Quantum wave-packet dynamics of H + HLi scattering: Reaction cross section and thermal rate constant. *J. Chem. Phys.* **121**, 7681–7691 (2004).
4. Wernli, M., Caruso, D., Bodo, E. & Gianturco, F. A. Computing a Three-Dimensional Electronic Energy Manifold for the LiH + H ↔ Li + H_2 Chemical Reaction. *J. Phys. Chem. A* **113**, 1121–1128 (2009).
5. Roy, T. & Mahapatra, S. Quantum dynamics of H + LiH reaction and its isotopic variants. *J. Chem. Phys.* **136**, 174313 (2012).
6. Carrasco, S. G. *et al*. State-to-state Quantum Wave Packet Dynamics of the LiH + H Reaction on Two Ab Initio Potential Energy Surfaces. *Astrophys. J.* **784**, 55 (2014).
7. Yuan, J., He, D. & Chen, M. A new potential energy surface for the ground electronic state of the LiH_2 system, and dynamics studies on the H(^{2}S) + LiH($X^1\Sigma^+$) → Li(^{2}S) + H_2($X^1\Sigma_g^+$) reaction. *Phys. Chem. Chem. Phys.* **17**, 11732–11739 (2015).
8. Prudente, F. V., Marques, J. M. C. & Maniero, A. M. Time-dependent wave packet calculation of the LiH plus H reactive scattering on a new potential energy surface. *Chem. Phys. Lett.* **474**, 18–22 (2009).
9. Liu, Y. F., He, X. H., Shi, D. H. & Sun, J. F. Stereodynamics of the reaction H + LiH($v = 0, j = 0$) → H_2 + Li and its isotopic variants. *Comput. Theor. Chem.* **965**, 107–113 (2011).
10. Clarke, N. J. *et al*. Classical and quantum dynamics on the collinear potential energy surface for the reaction of Li with H_2. *Chem. Phys.* **233**, 9–27 (1998).
11. Bililign, S., Kleiber, P. D., Kearney, W. R. & Sando, K. M. Reactive collision dynamics of Na*(4^2P) + H_2 and HD: Experiment and theory. *J. Chem. Phys.* **96**, 218–229 (1992).
12. Cavero, V., L'Hermite, J. M., Rahmat, G. & Vetter, R. Cs($6D_{3/2}$) + H_2 → CsH + H reaction. IV. Rotationally resolved total cross sections. *J. Chem. Phys.* **110**, 3428–3436 (1999).
13. Wong, T. H., Kleiber, P. D. & Yang, K. H. Chemical dynamics of the reaction K*($5p^2$P) + H_2 → KH($v = 0$; J) + H: Electronic orbital alignment effects. *J. Chem. Phys.* **110**, 6743–6748 (1999).
14. Fan, L. H., Chen, J. J., Lin, Y. Y. & Luh, W. T. Reaction of Rb(5^2D, 7^2S) with H_2. *J. Phys. Chem. A* **103**, 1300–1305 (1999).
15. Myers, E. G., Murnick, D. E. & Softky, W. R. Isotope Selective Laser Enhancement of the Li + H_2 Reaction. *Appl. Phys. B-Photo.* **43**, 247–251 (1987).
16. Bililign, S., Hattaway, B. C., Geum, N. & Jeung, G. H. Energy Transfer in Li*(3p)−H_2 Collisions. *J. Phys. Chem. A* **104**, 9454–9458 (2000).
17. Bililign, S., Hattaway, B. C., Robinson, T. L. & Jeung, G. H. Far-wing scattering studies on the reaction Li*(2p, 3p) + H_2 → LiH($v'' = 1$, 2, J'') + H. *J. Chem. Phys.* **114**, 7052–7058 (2001).
18. Chen, J. J. & Lin, K. C. Influence of vibrational excitation on the reaction Li($^{2\,2}$P$_J$) + H_2($v = 1$) → LiH($X^1\Sigma^+$) + H. *J. Chem. Phys.* **119**, 8785–8789 (2003).
19. Martínez, T. J. Ab initio molecular dynamics around a conical intersection: Li(2p) + H_2. *Chem. Phys. Lett.* **272**, 139–147 (1997).
20. Lee, H. S., Lee, Y. S. & Jeung, G. H. Potential energy surfaces for LiH_2 and photochemical reactions Li* + H_2 ↔ LiH + H. *J. Phys. Chem. A* **103**, 11080–11088 (1999).
21. Hsiao, M. K., Lin, K. C. & Hung, Y. M. Quasiclassical trajectory calculations for Li(2^2P$_J$) + H_2 → LiH($X^1\Sigma^+$) + H: Influence by vibrational excitation and translational energy. *J. Chem. Phys.* **134**, 034119 (2011).
22. He, D., Yuan, J., Li, H. & Chen, M. Global diabatic potential energy surfaces and quantum dynamical studies for the Li(2p) + H_2($X^1\Sigma_g^+$) → LiH($X^1\Sigma^+$) + H reaction. *Sci. Rep.* **6**, 25083 (2016).
23. Rackham, E. J., Gonzalez-Lezana, T. & Manolopoulos, D. E. A rigorous test of the statistical model for atom–diatom insertion reactions. *J. Chem. Phys.* **119**, 12895–12907 (2003).
24. Gamallo, P., Defazio, P. & González, M. Time Dependent Quantum Dynamics Study of the Ne + H_2^+($v_0 = 0$–4, $j_0 = 1$) → NeH^+ + H Proton Transfer Reaction, Including the Coriolis Coupling. A System with Oscillatory Cross Sections. *J. Phys. Chem. A* **115**, 11525–11530 (2011).
25. Gamallo, P., Huarte-Larrañaga, F. & González, M. Resonances in the Ne + H_2^+ → NeH^+ + H Proton-Transfer Reaction. *J. Phys. Chem. A* **117**, 5393–5400 (2013).
26. Larrégaray, P. & Bonnet, L. Quantum state-resolved differential cross sections for complex-forming chemical reactions: Asymmetry is the rule, symmetry the exception. *J. Chem. Phys.* **143**, 144113 (2015).
27. Bonnet, L., Larregaray, P. & Rayez, J. C. On the theory of complex-forming chemical reactions: effect of parity conservation on the polarization of differential cross sections. *Phys. Chem. Chem. Phys.* **9**, 3228–3240 (2007).
28. Polanyi, J. C. Concepts in reaction dynamics. *Acc. Chem. Res.* **5**, 161–168 (1972).
29. Yuan, J. C., He, D. & Chen, M. D. A new potential energy surface for the H_2S system and dynamics study on the S(^{1}D) + H_2($X^1\Sigma_g^+$) reaction. *Sci. Rep.* **5**, 14594 (2015).
30. Yuan, J. C., Cheng, D. H. & Chen, M. D. Time-dependent wave packet and quasiclassical trajectory studies of the Au plus HD reaction: competition between the reactive channels. *RSC. Adv.* **4**, 36189 (2014).
31. Zhang, D. H. & Zhang, J. Z. H. Full-dimensional time-dependent treatment for diatom-diatom reactions: The H_2 + OH reaction. *J. Chem. Phys.* **101**, 1146–1156 (1994).
32. Sun, Z., Zhang, D. H. & Alexander, M. H. Time-dependent wavepacket investigation of state-to-state reactive scattering of Cl with para-H_2 including the open-shell character of the Cl atom. *J. Chem. Phys.* **132**, 034308 (2010).
33. Cheng, D. H., Yuan, J. C. & Chen, M. D. State-Resolved Time-Dependent Wave Packet and Quasiclassical Trajectory Studies of the Adiabatic Reaction S(^{3}P) + HD on the (1^3A″) State. *J. Phys. Chem. A* **118**, 55–61 (2014).

34. Aguado, A., Paniagua, M., Lara, M. & Roncero, O. Potential energy surface and wave packet calculations on the Li + HF → LiF + H reaction. *J. Chem. Phys.* **106**, 1013–1025 (1997).
35. Li, W. T., Chen, M. D. & Sun, Z. G. Quantum Dynamics of Li + HF/DF Reaction Investigated by a State-to-State Time-dependent Wave Packet Approach. *Chin. J. Chem. Phys.* **28**, 415–425 (2015).
36. Sun, Z. G., Lin, X., Lee, S. Y. & Zhang, D. H. A Reactant-Coordinate-Based Time-Dependent Wave Packet Method for Triatomic State-to-State Reaction Dynamics: Application to the H + O_2 Reaction. *J. Phys. Chem. A* **113**, 4145 (2009).
37. Sun, Z. G., Lee, S. Y., Guo, H. & Zhang, D. H. Comparison of second-order split operator and Chebyshev propagator in wave packet based state-to-state reactive scattering calculations. *J. Chem. Phys.* **130**, 174102 (2009).

Acknowledgements

This work was supported by the National Natural Science Foundation of China (Grant No. 11374045), and Program for New Century Excellent Talents in University (Grant No. NCET-12-0077).

Author Contributions

M. Chen supervised the project, D. He calculated the ab initio energy points, J. Yuan fitted the potential energy surface and performed the time-dependent wave packet calculations, D. He and M. Chen wrote the paper.

Additional Information

Competing Interests: The authors declare that they have no competing interests.

Publisher's note: Springer Nature remains neutral with regard to jurisdictional claims in published maps and institutional affiliations.